ACI STRUCTURAL JOURNAL TECHNICAL PAPER

Title no. 98-S47

Influence of Concrete Strength and Transverse Reinforcement Yield Strength on Behavior of High-Strength Concrete Columns

by Patrick Paultre, Frédéric Légeron, and Daniel Mongeau

Eight large-scale high-strength concrete (HSC) square columns were constructed and tested under simulated earthquake loading. The concrete strength varied from 80 to 120 MPa. The columns were subjected to constant axial loads corresponding to 40 and 52% of the columns' axial load capacity and to a cyclic horizontal load-inducing reversed bending moment. It is shown that, at constant volumetric ratio of confinement reinforcement and constant level of axial compression, concrete strength significantly influences the flexural behavior of HSC columns. It is also shown that, in some cases, high-yield-strength reinforcement may be used to effectively confine HSC while reducing the volumetric ratio of lateral transverse reinforcement. This highlights the need for a reliable index to account for high-yield-strength transverse reinforcement. The test results from this research program and others indicate that the confinement reinforcement requirements of the ACI and New Zealand Codes are not directly applicable to columns confined with high-yield-strength steel.

Keywords: confined concrete; ductility; high-strength concrete; high-strength steel; tied column.

INTRODUCTION

High-strength concrete (HSC) offers many advantages such as enhanced mechanical performance and durability, in addition to member size reduction. Because of its more brittle behavior in compression than normal-strength concrete (NSC), HSC has been slow to gain acceptance in seismically active regions. Some concrete design codes even limit the maximum strength that can be used for seismic designs. For example, the New Zealand Code[1] limits concrete compressive strength to 100 MPa for ordinary concrete structures, compared with 70 MPa for ductile structures; the corresponding limits are 80 and 50 MPa in Canada.[2] ACI Code 318[3] does not limit concrete compressive strength; however, its confinement requirements were originally derived from experimental results from NSC and are not adapted to HSC columns.[4-6] Nonetheless, it has been shown[4-9] that HSC columns reinforced according to current code requirements behave in a ductile manner if the axial load is less than 20% of the columns' axial load capacity, measured as $A_g f_c'$, where A_g is the gross concrete cross section and f_c' is the concrete strength. When concrete strength increases, the amount of confinement reinforcement has to be increased to reach a constant level of ductility for columns subjected to the same level of axial load. For columns subjected to a high level of axial load, large amounts of confinement reinforcement may be necessary to achieve the ductility required in seismically active areas. This high amount of lateral steel results in congestion of reinforcing cages and concreting problems. Increasing the yield strength of transverse reinforcement steel has been suggested to lower the amount of transverse reinforcement. Yet increasing the yield strength of confinement steel does not necessarily result in increased ductility when lateral steel content is kept constant.[4] Other experimental investigations have concluded that high-yield-strength steel (HYSS) may be partially effective.[5] It should be noted that the New Zealand Code[1] allows the use of HYSS to a maximum of 800 MPa.

The test program reported in this paper is part of a comprehensive research program on the behavior of HSC confined columns. The aim of this research program is to explain the mechanism of confinement through a simplified but rational approach.[10,11] In the first part of this work, high-strength self-compacting concrete, fiber-reinforced high-strength concrete (FRHSC), and HSC columns were tested under concentric compression.[12-14] A confinement model, based on equilibrium and strain compatibility and accounting for the true transverse reinforcement stress at peak strength, has been developed and calibrated to available test data on large-scale columns.[10,11] To complete this work, tests on HSC columns subjected to combined constant axial load and reversed cyclic flexure simulating earthquake loading were performed on 21 large-scale FRHSC and HSC columns. In one of the test series,[9] the effect of two parameters (the level of axial compression and the volumetric ratio of confinement reinforcement) were studied. This test series concentrates on the effects of two additional but important parameters: concrete strength and the yield strength of the confinement steel.

RESEARCH SIGNIFICANCE

This paper presents new test data on the behavior of HSC columns under simulated earthquake loading. Eight HSC column specimens were subjected to combined constant axial load and reversed cyclic flexure. The target concrete strength was 80, 100, and 120 MPa. The influence of concrete strength and the transverse reinforcement steel ratio and yield strength are investigated. The objective of this work is to evaluate the ability of HYSS to confine HSC columns so as to lower the amount of transverse reinforcement of very congested reinforcing cages. For this purpose, a confinement index must be defined because the volumetric ratio of transverse reinforcement is not sufficient to compare columns confined with transverse steel having different yield strengths. ACI-ASCE Committee 441[7] recommended the ratio $\rho_s f_{yh}/f_c'$, referred to hereafter as the confinement index I_c, where ρ_s is

ACI Structural Journal, V. 98, No. 4, July-August 2001.

ACI member **Patrick Paultre** *is a professor of structural engineering at the University of Sherbrooke, Sherbrooke, Quebec, Canada. He is a member of Joint ACI-ASCE Committees 352, Joints and Connections in Monolithic Concrete Structures, and 441, Reinforced Concrete Columns.*

ACI member **Frédéric Légeron** *is a bridge engineer at J. Muller International, New York. He received his PhD from the University of Sherbrooke and École Nationale des Ponts et Chaussées, Paris, France. He is the former treasurer of the Paris ACI chapter. His research interests include the seismic design of bridges and nonlinear analysis of reinforced and prestressed concrete structures.*

Daniel Mongeau *is a structural engineer at Canam-Manac Group, Boucherville, Quebec, Canada. He received his MScA from the University of Sherbrooke.*

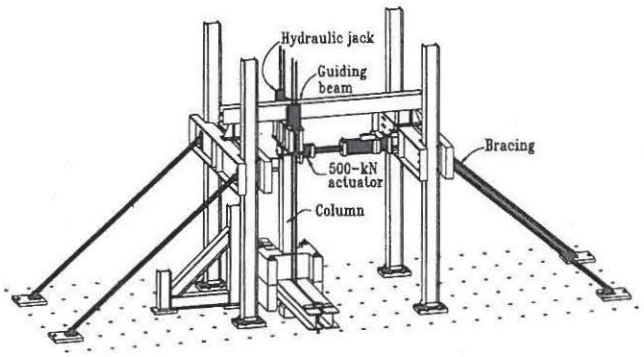

Fig. 1—Experimental setup.

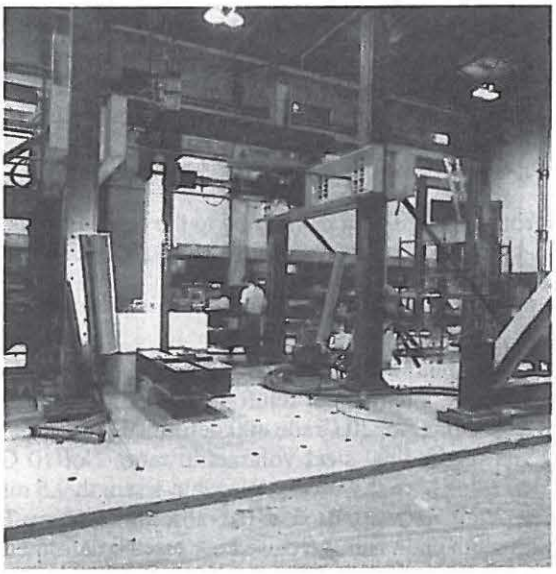

Fig. 2—Photograph of experimental setup and testing frame.

the volumetric ratio of confinement steel, f_{yh} is the yield strength of the confinement steel, and f'_c is concrete strength. This index is evaluated in this paper together with the effective confinement index I_e proposed by Cusson and Paultre.[10] The effectiveness of the confinement reinforcement requirements of the ACI and New Zealand Codes are also discussed.

EXPERIMENTAL PROGRAM

Test specimens

The specimens tested in this research program consisted of six 305 x 305 x 2150 mm columns connected to a massive I-shaped stub and cast vertically. These specimens have the same geometry as the other two specimens reported elsewhere.[9] The test setup is shown in Fig. 1 and 2. A varying transverse load was applied to the tip of the specimens at 2.00 m from the base of the column with a force/displacement-controlled hydraulic actuator. The specimens could be thought of as a 4.00 m high column in a typical building with the point of contraflexure located at midheight of the column. Figure 3 shows the reinforcement details and the tie configuration of the specimens. The test results of two similar column specimens that are part of another test series[9] are also presented for comparison.

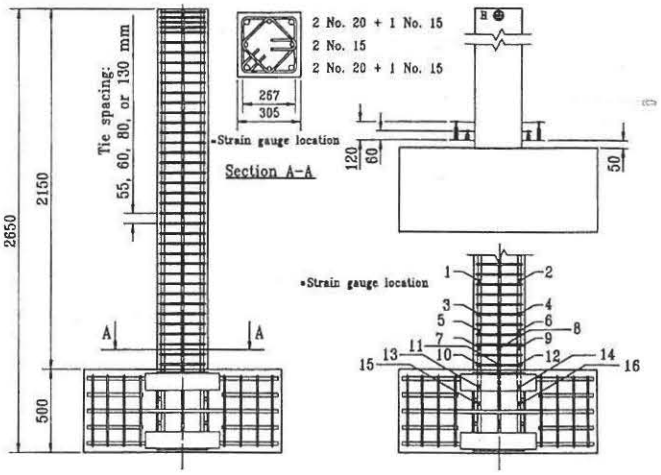

Fig. 3—Reinforcing cage and instrumentation details.

Test variables

The test series reported on here were designed to investigate two main parameters influencing the behavior of columns: 1) the concrete compressive strength; and 2) the transverse reinforcement amount and its yield strength. The second variable was investigated for two levels of axial load measured as the ratio of the constant applied compression P and the column gross concrete axial load capacity $A_g f'_c$. The compressive force was applied to the tip of the column specimens and kept constant at 2900, 3600, 4200, and 5150 kN. Considering that the targeted concrete strengths were 80, 100, and 120 MPa, these axial loads correspond to target axial load levels of 40 and 52%. The high axial load levels were selected primarily to ensure that failure would occur by concrete crushing above the balanced point. This condition places high ductility demands on columns usually located in the lower stories, where they are highly loaded axially, and is of paramount importance in ductile seismic design. It is also expected that stress in confining steel would increase as the axial load level increases to the point at which HYSS becomes more effective.

To investigate the influence of the yield strength and amount of confinement steel, the tie configuration was kept constant, but the tie spacing varied from 55 to 60 to 80 to 130 mm. Five columns were confined with 11.3 mm diameter Grade 400 steel. For these column specimens, a 130 mm tie spacing corresponds to a normal shear design controlled by the ACI Code[3] $d/2$ requirement. The 60 mm tie spacing was selected to obtain ductile behavior, even at high axial load levels, and represents about 95% of the confinement steel required by the ACI Code for this steel grade. Three columns were confined with 9.5 mm diameter grade 800 steel. For these columns, a spacing of 80 mm is required to obtain the same confinement index as with similar ties made with 11.3 mm diameter Grade 400 steel at 60 mm spacing. A spacing of 55 mm with 9.5 mm diameter Grade 800 confinement steel gives an effective confinement index as proposed

Table 1—Concrete characteristics

Specimen	f_c', MPa	ε_c'	E_c, MPa	ε_{c50u}	f_r, MPa
C80B60N40	78.7	0.0030	35,800	0.0044	6.96
C100B60N40	98.2	0.0033	35,600	0.0043	8.33
C120B60N40	109.2	0.0035	38,200	—	8.73
C100B130N40	104.3	0.0033	37,600	0.0041	9.04
C100BH55N40	109.5	0.0033	39,600	—	9.34
C100BH80N40	104.2	0.0033	39,300	—	8.87
C100BH55N52	104.5	0.0034	38,100	—	7.29
C100B60N52	109.4	0.0033	39,200	—	8.13

by Cusson and Paultre[10] and Paultre and Légeron[11] similar to a column specimen reinforced with 11.3 mm diameter Grade 400 confinement steel spaced at 60 mm.

Each specimen is identified by a string of characters beginning with the concrete strength (C80, C100, C120) followed by the steel configuration and grade (B for the Grade 400 diamond-shape tie configuration as defined by Cusson and Paultre[12] and BH for a similar configuration with Grade 800 confinement steel), the tie spacing in millimeters (55, 60, 80, or 130), and the letter N followed by the target axial load level in percent of $A_g f_c'$ (40 or 52). Hence, C100BH55N40 refers to the column specimen made of 100 MPa concrete with tie configuration B and Grade 800 confinement steel, spaced at 55 mm, and subjected to 40% of $A_g f_c'$.

Material properties

The specified 80, 100, and 120 MPa concretes were mixed in-house. The concrete formulation was based on water-cement ratios (w/c) of 0.24 for 120 MPa, 0.25 for 100 MPa, and 0.35 for 80 MPa. For the 80 and 100 MPa concrete, the same Type 10SF Canadian Lafarge cement was used. The cement was premixed with silica fume (7.5 ± 0.5% of the total weight of cement and silica fume). Type 30 Canadian Saint Lawrence cement was used for the 120 MPa concrete. In this case, the silica fume was added during mixing. The concrete formulations were similar to those used by Cusson and Paultre.[12] Casting of the specimens followed the same procedure reported by Légeron and Paultre.[9] All the control cylinders and prisms were cured under the same conditions as the column specimen to estimate the column concrete characteristics as accurately as possible.

Table 1 summarizes the measured material properties. The concrete compressive strength f_c' was determined from standard compressive tests on at least three 150 x 300 mm cylinders. Complete stress-strain curves were obtained from at least three 100 x 200 mm cylinders tested under displacement control at a very slow strain rate in a very stiff testing machine. The postpeak strain at 50% of maximum stress ε_{c50u} was evaluated from the complete stress-strain curves obtained on 100 x 200 mm cylinders. Even with the slow strain rate used and the small cylinder size, it was not possible to measure the complete stress-strain curve on most of the higher strength concrete.

Four different types of reinforcing bars were used: 10M (100 mm^2), 15M (200 mm^2), and 20M (300 mm^2) Grade 400 bars, and 9.5 mm diameter Grade 800 bars. Complete stress-strain curves were obtained from test coupons on each of the steel batches used. The average of at least three steel coupons for each batch of steel are shown in Table 2, where f_y is the yield strength; ε_{sh} is the commencement of strain hardening; and ε_{su} is the ultimate strain corresponding to the ultimate stress, f_{su}. All the steels exhibited a well-defined yield plateau from the beginning of yielding to the commencement of strain-hardening, except from high-yield-strength steels that presented a rounded stress-strain curve.

Table 2—Steel characteristics

	Specimen	f_y, MPa	ε_{sh}	ε_{su}	f_{su}, MPa
No. 10M and 9.5d	C80B60N40	438*	0.0123	0.136	689
	C100B60N40	418*	0.0127	0.138	675
	C120B60N40	438*	0.0123	0.136	689
	C100B130N40	418*	0.0127	0.138	675
	C100BH55N40	825†	—	0.062	960
	C100BH80N40	825†	—	0.062	960
	C100BH55N52	744†	—	0.067	874
	C100B60N52	492†	—	0.104	715
No. 15M	C80B60N40	499	0.0038	0.094	734
	C100B60N40	467	0.0109	0.100	722
	C120B60N40	499	0.0038	0.094	734
	C100B130N40	467	0.0109	0.100	722
	C100BH55N40	499	0.0038	0.094	734
	C100BH80N40	499	0.0038	0.094	734
	C100BH55N52	533	0.0150	0.125	728
	C100B60N52	533	0.0150	0.125	728
No. 20M	C80B60N40	446	0.0064	0.106	719
	C100B60N40	451	0.0065	0.109	716
	C120B60N40	446	0.0064	0.106	719
	C100B130N40	451	0.0065	0.109	716
	C100BH55N40	446	00064	0.106	719
	C100BH80N40	446	00064	0.106	719
	C100BH55N52	446	00064	0.106	719
	C100B60N52	446	00064	0.106	719

*No. 10M Grade 400 MPa steel.
†9.5d Grade 800 MPa steel, 0.2% yield strength with no yield plateau.

Reinforcing cages

Details of reinforcing cages are shown in Fig. 3. For each specimen, the longitudinal reinforcement consisted of four No. 15 and four No. 20 Grade 400 deformed bars, providing a 2.15% longitudinal steel volumetric ratio. No. 10 Grade 400 deformed bars as well as high-yield-strength 9.5 mm diameter plain bars were used as lateral reinforcement. These high-strength plain bars were used because no deformed bars with sufficiently high yield strength were available. To prevent crushing of the concrete, extra ties were placed at the top of the columns where the axial load was applied; elsewhere, ties were equally spaced. Anchorage length of ties was 110 mm for the No. 10 bars and 100 mm for the 9.5 mm diameter bars to meet the seismic requirements of the ACI Code. No tie anchorage failure was observed during the test. The stub was designed to prevent excessive cracking and provide sufficient anchorage for the column's longitudinal bars.

Instrumentation

For each specimen, 16 electrical strain gages were placed on the longitudinal bars above and in the stub (Fig. 3). Four sets of ties just above the stub were also instrumented with 16 electrical strain gages. Two sets of four linear variable displacement transducers (LVDTs) were placed in the plastic hinge region on two lateral faces of the columns parallel to the plane of loading. The LVDTs were supported by steel

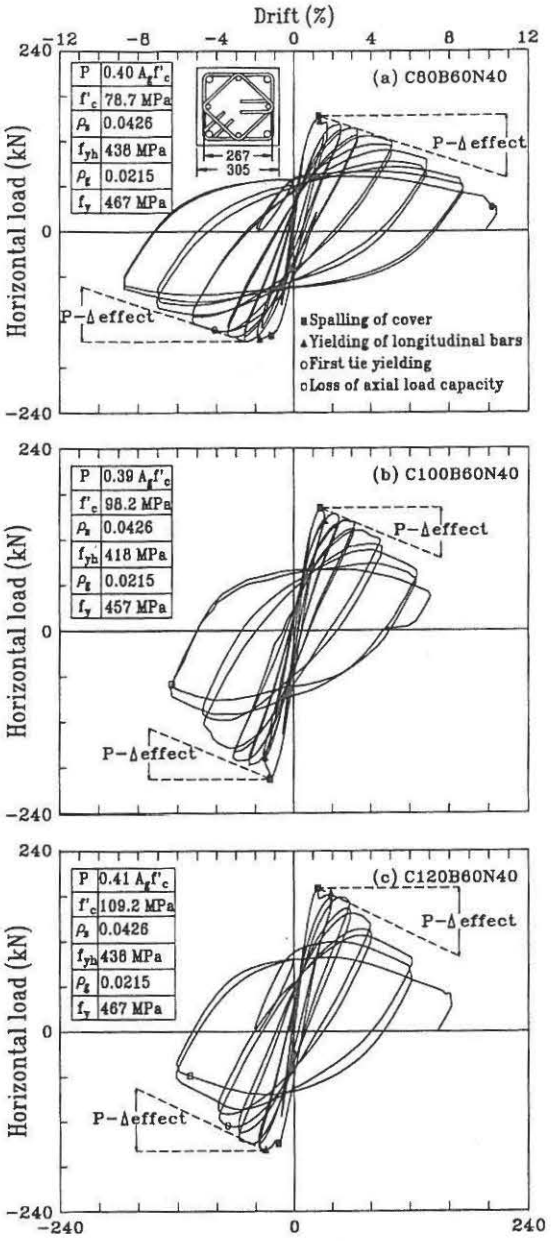

Fig. 4—Uncorrected lateral load versus tip displacement for Specimens C80B60N40, C100B60N40, and C120B60N40.

rods passing through the core and extending from one side of the column to the other. These LVDTs were attached to the longitudinal bars before concreting. Four LVDTs with a range of 5 mm were used to measure average concrete strain over a gage length of 60 mm. Four other LVDTs with a range of 25 mm were placed over these four LVDTs to measure over a longer gage length of 120 mm (Fig. 3). The Dywidag bars used to apply the axial load were instrumented and calibrated to measure the applied load. The applied horizontal load was measured by the load cell on the actuator, which was also equipped with an LVDT to control the actuator while in displacement control mode. The horizontal tip displacement was measured by an LVDT with a range of 300 mm. This LVDT was mounted to a braced bracket fixed to the strong slab to have a displacement measure independent of testing frame movement. Due to the frame's high stiffness, the difference between the actuator LVDT and the independent LVDT did not exceed a few millimeters. All the experimental data were stored at predetermined steps and recorded at special occurrences such as cracking, yielding, and zero crossing. Acquisition was performed by increments of force during the force-controlled phase and displacement triggers during the displacement-controlled phase.

Experimental frame and testing procedure

The testing frame was specially designed for this research program (Fig. 1 and 2). The axial compression in the column was induced by six high-strength 36 mm diameter post-tensioning bars tensioned by two 1000 kN and four 1500 kN hydraulic jacks. The horizontal load was applied by a 500 kN tension/compression actuator with displacement and force control capabilities, supported by four braced steel columns. The axial load was first applied at the target value. The horizontal force was applied under force control to a maximum value corresponding to 75% of the predicted analytical yield load. The second cycle started under displacement control and reached the yield load defined as the point at which the longitudinal bar first yielded in tension, which also marked the yield displacement. Thereafter, each cycle was under displacement control with a maximum displacement equal to 1.5, 2, 3, ... times the experienced yield displacement up to failure. Except for the first cycle, whose sole purpose was to crack the member to simulate service conditions and obtain elastic characteristics, all subsequent cycles were repeated twice. During the test, the axial load was maintained constant by readjusting the tension in the post-tensioning bars after each half cycle. The test ended when at least one of the following three events occurred: 1) the column was not able to sustain axial load, characterized by a 10% loss of axial load during a quarter of a cycle; 2) flexural resistance dropped more than 50% of the maximum experienced capacity; or 3) a longitudinal bar ruptured, inducing a large drop in flexural capacity.

TEST RESULTS

General behavior

The experimentally measured lateral load-tip deflection responses are presented in Fig. 4 and 5. The lateral load is reported as measured and not corrected for the P-Δ effect, which is indicated by the dotted line. A strength gain occurs when the response curve, in absolute terms, lies above the oblique P-Δ dotted line. A strength loss is obtained when the response curve is under the P-Δ line. Occurrences of special events such as spalling of cover concrete, yielding of ties, and yielding and buckling of longitudinal bars are indicated in the figures.

Table 3 summarizes the experimental results obtained for each specimen. It includes the concrete compressive strength f'_c for each specimen, the volumetric ratio ρ_s of confinement steel to concrete core delineated by the centerline of the perimeter ties, and the average yield strength of ties f_{yh}. The ratio $P/A_g f'_c$ of the applied axial load P over the concrete gross section capacity $A_g f'_c$ ranged from 0.35 to 0.51. These values are compared with the ratio P/P_0 of the applied axial load over the nominal concentric compression capacity, $P_0 = 0.85 f'_c (A_g - A_{st}) + A_{st} f_y$, and ranged from 0.38 to 0.55. For each column, the main indexes quantifying the specimen behavior are summarized in Table 3. The meaning of the indexes will be discussed in following paragraphs.

All specimens experienced failure by concrete crushing; some longitudinal bars buckled slightly. C100B130N40 had two large diagonal cracks in the damaged zone and exhibited

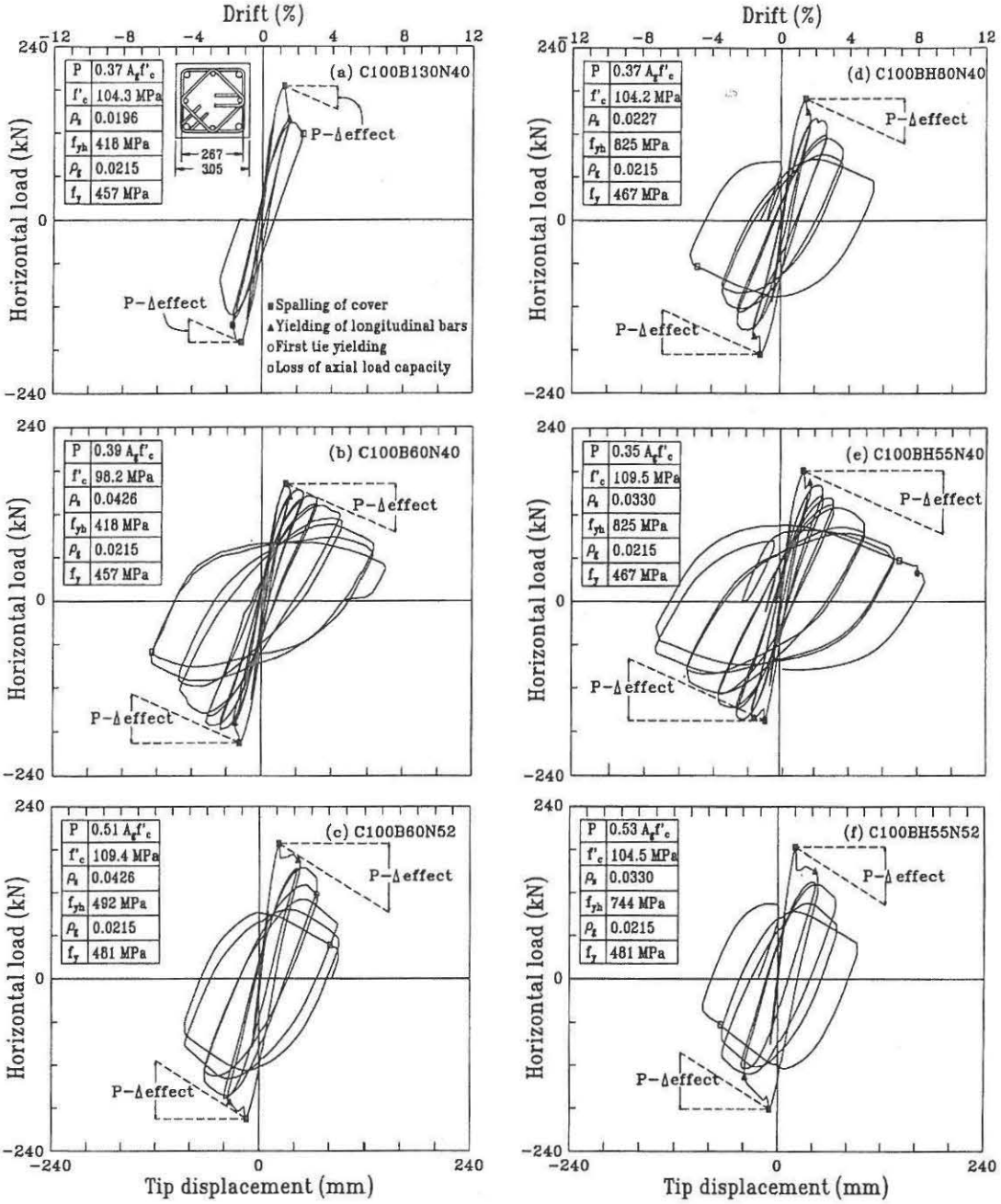

Fig. 5—Uncorrected lateral load versus tip displacement for Specimens C100B130N40, C100B60N40, C100B60N52, C100BH80N40, C100BH55N40, and C100BH55N52.

very brittle behavior. Specimen C100BH80N40 experienced also a very brittle failure but without any visible diagonal cracking.

Figure 6 shows the appearance of the specimens at the end of the test. All the columns were heavily damaged just above the base stub. The length of the damaged region extended about two to three times the column depth. The extent of the damage zone measured is consistent with observations made by others on NSC and HSC columns.[9,15] In all the specimens, however, sections just above the stub were not damaged, although they were subjected to the maximum moment (Fig. 7). The same phenomenon were observed on similar specimens by other researchers.[5,8,9,16] Tanaka, Park, and McNamee[17] and later Sheikh and Rhoury[16] attributed such behavior primarily to confinement provided by the base stub to the sections in its immediate vicinity. Such confinement increases actual moment capacity of the sections just above the stub. This length of undamaged concrete corresponds approximately to the spacing between the column-stub interface and the first hoop and had an average value of about 40 mm for all eight specimens. Therefore, the resisting moment M'_{max} reported in Table 3 is calculated 40 mm above the column-stub interface.

The cover concrete spalled off before yielding of longitudinal bars. A loud noise occurred when the cover concrete spalled off suddenly, as the capacity of the column dropped sharply. In the case of C100B130N40, with a 37% axial load level, the flexural capacity dropped by about 20%. For the other specimens, loss of flexural capacity was slightly smaller, though similar. Specimens did not exhibit any warning sign, such as vertical cracking, prior to spalling. The splitting plane between cover and core concrete was found to be quite

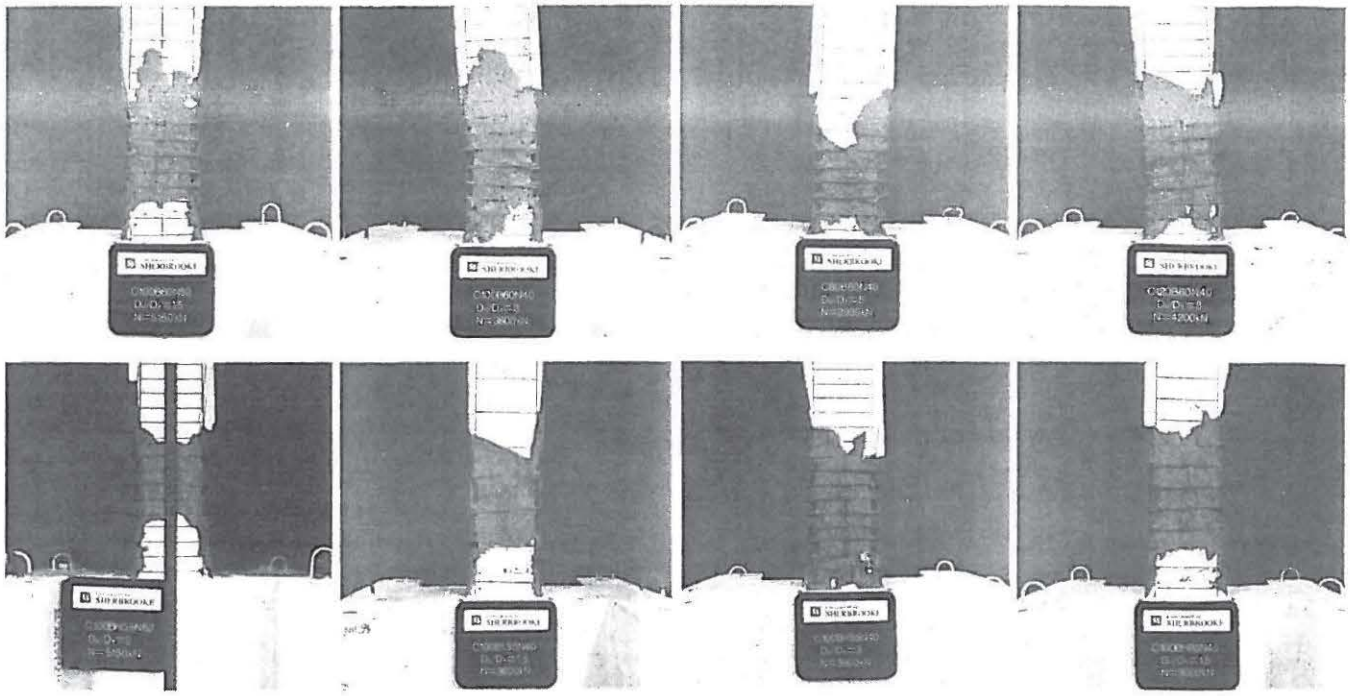

Fig. 6—Photographs of damaged regions and plastic hinge zones for all specimens.

Table 3—Summary of results

Specimen	f_c', MPa	ρ_s	f_{yh}, MPa	$\rho_s f_{yh}/f_c'$	$\rho_s A_g/f_c'$	P/P_0	M'_{max}, kNm	$\mu_{\Delta u}$	$\mu_{\phi u}$	E_N	I_W	D_{EW}
C80B60N40	78.7	0.0426	438	0.237	0.40	0.41	329.7	10.1	32.4	66.9	35.2	348.1
C100B60N40	98.2	0.0426	418	0.181	0.39	0.42	377.4	5.2	7.6	33.8	22.5	114.2
C120B60N40	109.2	0.0426	438	0.171	0.41	0.45	388.3	4.7	5.2	26.2	15.9	75.0
C100B130N40	104.3	0.0196	118	0.079	0.37	0.40	172.6	1.6	2.9	4.2	3.3	5.6
C100BH55N40	109.5	0.0330	825	0.248	0.35	0.38	379.5	5.4	8.0	21.0	15.3	57.5
C100BH80N40	104.2	0.0227	825	0.179	0.37	0.40	379.9	2.6	4.6	4.2	3.7	6.7
C100BH55N52	104.5	0.0330	744	0.235	0.53	0.57	386.1	2.8	—	10.6	4.5	223.1
C100B60N52	109.4	0.0426	492	0.192	0.51	0.55	410.5	3.6	5.7	20.7	10.0	53.0

smooth due to cracks passing through and fracturing the aggregates. No tie failed during the test. Average strains in the confinement steel ranged from 0.001 to 0.006 m/m in all the specimens. These measured strains accounts for both shear strains and confinement strains and are reported elsewhere.[18]

Ductility and energy dissipation

Seismic response indicators are generally quantified by curvature and structural ductility and by energy-dissipation capacity. Structural ductility can be somewhat directly related to the seismic force reduction factor used in most codes to calculate the seismic base shear.[19] Energy-dissipation capacity is a better parameter to use in the design of short-period structures and structures subjected to long-duration earthquakes. All three indicators are evaluated in this paper to compare the column behavior on rational bases.

Ductility parameters are defined from an idealized diagram[16,20] because the response of a reinforced concrete column is far from bilinear. Hence, the load-displacement behavior is idealized as a bilinear diagram, constituted of an elastic branch and an inclined inelastic branch (Fig. 8(a)). The elastic branch crosses the experimental curve at 75% of maximum horizontal load and reaches the maximum horizontal load to define the idealized yield displacement Δ_{yI}. Failure of the column is defined conventionally when the postpeak displacement Δ_2 reaches a point at which the remaining column strength has dropped to 80% of the maximum experienced load. The idealized postelastic branch joins the point (Δ_{yI}, H_{max}) to the point (Δ_2,H_2), where H_2 is calculated by equating the areas under the idealized diagram and the experimental envelope curve, thus ensuring equal energy criteria. The sectional behavior in terms of moment-curvature diagrams is idealized with a similar procedure (Fig. 8(b)). The ductility parameters are calculated from the idealized diagrams. The ultimate displacement ductility is defined as

$$\mu_{\Delta u} = \frac{\Delta_2}{\Delta_{yI}} \tag{1}$$

and the ultimate curvature ductility as

$$\mu_{\phi u} = \frac{\phi_2}{\phi_{yI}} \tag{2}$$

The displacement ductility $\mu_{\Delta u}$ and curvature ductility $\mu_{\phi u}$ for each column are given in Table 3. It is evident that these ductility parameters can have different values, depending on the definition of the yield point and ultimate point in the ide-

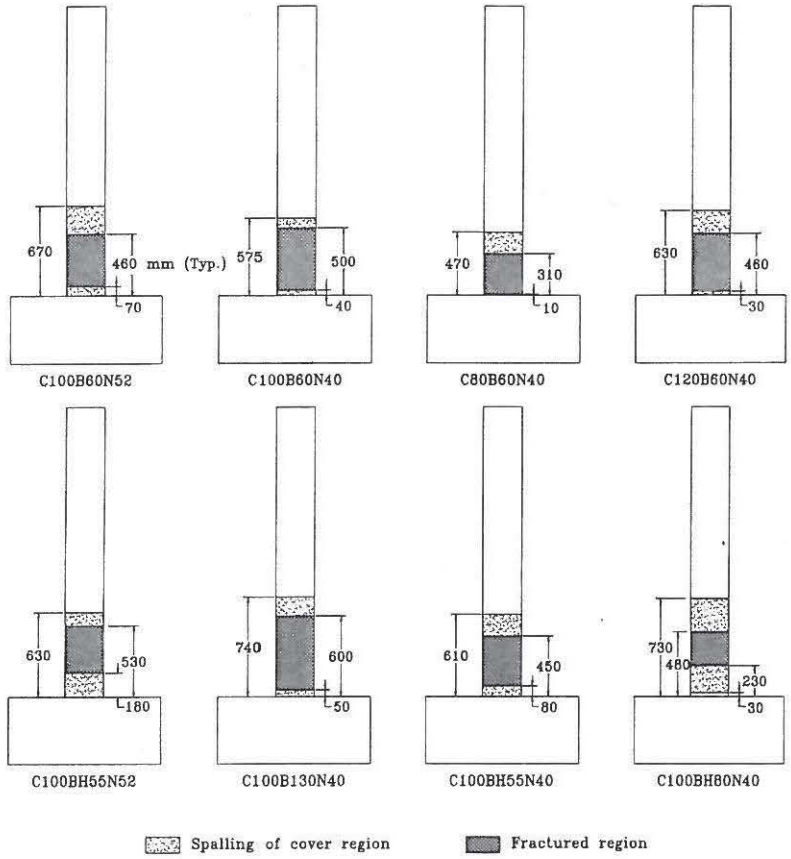

Fig. 7—Diagrams of most damaged regions of specimens.

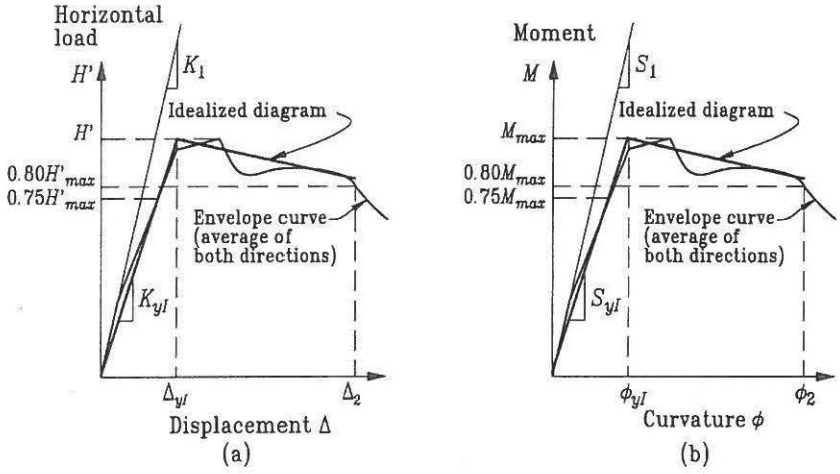

Fig. 8—Ideal curve definitions: (a) horizontal load versus displacement; and (b) moment versus curvature.

alized diagram. The maximum interstory drift ratio δ_u is a more direct parameter to define, as it is based on the measured displacement at failure

$$\delta_u = \frac{\Delta_2}{z} \tag{3}$$

where the column height z = 2000 mm. This parameter takes into account both the inelastic and elastic behavior. It is generally assumed that a drift ratio of about 4% represents a very good level of ductility.[7] The interstory drift ratio is reported on the top horizontal axes in Fig. 4 and 5.

The energy dissipation is defined for cycle i by the hatched area in Fig. 9 or mathematically by

$$E_i = \oint_A^B F du \tag{4}$$

The total energy dissipated during the test until 80% conventional failure is reached is

$$E_{hyst} = \sum_{i=1}^{n} E_i \tag{5}$$

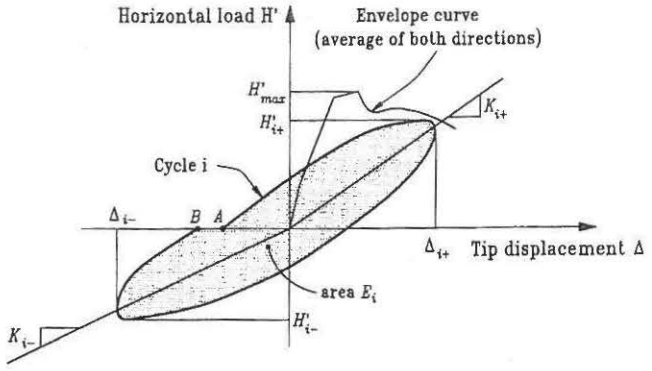

$$\Delta_i = 1/2\,(\Delta_{i+1}+\Delta_{i-1})$$

$$H_{i,max} = 1/2\,(H_{i+1}+H_{i-1})$$

$$K_i = 1/2\,(K_{i+1}+K_{i-1})$$

Fig. 9—Energy dissipation.

where n is the number of cycles to failure. For comparison purposes, it is convenient to normalize the dissipated energy as

$$E_N = \frac{1}{H'_{max}\Delta_{yI}}\sum_{i=1}^{n} E_i \tag{6}$$

where E_N is the normalized dissipated energy and H' is the applied horizontal load H added to the equivalent horizontal load due to the P-Δ effect. Only cycles occurring before conventional failure are taken into account in determining E_N, which is reported in Table 3 for each specimen.

Energy dissipation and inelastic deformation capabilities may also be assessed by work and damage indexes. The work index I_W proposed by Gosain, Brown, and Jirsa[21] is reported in Table 3 and is defined as

$$I_W = \sum_{i=1}^{n} \frac{H_i\Delta_i}{H'_{max}\,\Delta_{yI}} \tag{7}$$

Table 3 also gives the damage index D_{EW} proposed by Ehsani and Wright,[22] which combines the cyclic dissipated energy and the elastic energy

$$D_{EW} = \frac{1}{H'_{max}\,\Delta_{yI}}\sum_{i=1}^{n} E_i\left(\frac{K_i}{K_{yI}}\right)\left(\frac{\Delta_i}{\Delta_{yI}}\right)^2 \tag{8}$$

where K_i and Δ_i are defined in Fig. 9.

ANALYSIS OF RESULTS

Two parameters are investigated in this research program: the effect of the concrete strength and the effect of the lateral steel content and yield strength. The effect of concrete strength can be assessed in Fig. 4, while the effect of the lateral steel content and yield strength can be assessed in Fig. 5. In Fig. 4, the responses of Specimens C80B60N40, C100B60N40, and C120B60N40 are arranged in three rows by ascending concrete strength from top to bottom. In Fig. 5, the response of Specimens C100B130N40, C100BH80N40, C100B60N40, C100BH55N40, C100B60N52, and C100BH55N52 are arranged in three rows and two columns. The left column in this figure presents the cyclic force-displacement responses of specimens reinforced with lateral reinforcement made of normal-yield-strength steel, while the right column corresponds to specimens reinforced with HYSS. Specimens tested under 40% axial load level are displayed in the first two rows. The two specimens tested under 52% axial load level are provided in the last row.

Effect of concrete compressive strength

The influence of the concrete compressive strength can be observed in the response curves for Specimens C80B60N40, C100B60N40, and C120B60N40 presented in Fig. 4. The geometry and amount of the confinement steel is identical for all three columns, which were made with concrete with compressive strength of 78.7, 98.2, and 109.2 MPa (80, 100, and 120 MPa target compressive strength), respectively. The three columns were tested under 40, 39, and 41% axial load level (target axial load level of 40%), respectively. It can be clearly seen from this figure that, when concrete strength increases, the capacity to sustain large inelastic displacement decreases sharply. The ductility parameters and energy-dissipation capacity for the three specimens are reported in Table 3 in which the specimens are grouped in ascending order of concrete strength. The displacement ductility drops from 10.1 to 5.2 and 4.7 when the concrete strength increases from 78.7 to 98.2 and 109.2 MPa. The same influence is observed in the other indicators: the curvature ductility; the normalized dissipated energy E_N; the work index I_W; and the damage index D_{EW}.

For design purposes, a simple index is useful to evaluate the influence of concrete strength. The factor $\rho_s f_{yh}/f'_c$ (called herein confinement index I_c) has been recommended by ACI-ASCE Committee 441[7] to evaluate confinement efficiency. This index is given in Table 3 for Columns C80B60N40, C100B60N40, and C120B60N40. Although the relation between $\rho_s f_{yh}/f'_c$ and the displacement ductility is not linear, this index correlates reasonably with ductility and energy indexes: the specimen with the highest value of $\rho_s f_{yh}/f'_c$ behaves in the most ductile manner. It is therefore appropriate to use this index to compare the displacement capacity of columns made of concrete of different strengths but tested at the same level of axial load and with the same lateral steel content and yield strength. As will be shown in following paragraphs, this index is not appropriate when comparing columns under different axial load levels or reinforced with steel with different yield strengths.

Effect of lateral steel content and yield strength

The influence of the amount of lateral reinforcement has been assessed in a previous paper.[9] In this research program, the possibility of replacing normal yield-strength steel by HYSS is evaluated. As mentioned previously, HSC columns subjected to high axial loads may require a very high amount of lateral reinforcement. This congests the reinforcing cage, resulting in concreting problems. It is believed that the same level of ductility can be achieved with a lower amount of confinement steel when HYSS is used; however, earlier investigation showed that the use of HYSS may not be efficient for every column configuration.[4,5]

Part of this research program was designed to assess the efficiency of the confinement index $\rho_s f_{yh}/f'_c$ in predicting the displacement capacity of confined HSC columns. Three sets of columns are used to evaluate the influence of the confinement index. The results are presented in Table 4 grouped by set and in ascending order of $\rho_s f_{yh}/f'_c$. The first set groups to-

Table 4—Influence of $\rho_s f_{yh}/f_c'$ index

Specimen	$\rho_s f_{yh}/f_c'$	$\mu_{\Delta u}$	$\mu_{\phi u}$	$\delta_{\theta u}$	E_N	D_{EW}	I_W
C100B130N40	0.079	2.9	1.6	1.5	4.2	3.3	5.6
C100BH80N40	0.179	4.6	2.6	2.4	4.2	3.7	6.7
C100B60N40	0.181	7.6	5.2	5.1	33.8	22.5	114.2
C100CH55N40	0.248	8.0	5.4	4.8	21.0	15.3	57.5
C100BH55N52	0.235	—	2.8	2.3	10.6	4.5	223.1
C100B60N52	0.192	5.7	3.6	3.4	20.7	10.0	53.0
C120B60N40	0.171	5.2	4.7	5.0	26.2	15.9	75.0
C100BH80N40	0.179	4.6	2.6	2.4	4.2	3.7	6.7
C80B60N40	0.237	32.4	10.1	8.9	66.9	35.2	348.1
C100BH55N40	0.248	8.0	5.4	4.8	21.0	15.3	57.5

gether four columns: C100B130N40, C100BH80N40, C100B60N40, and C100BH55N40. The four columns were subjected to the same axial load level and had confinement index values ranging from 0.079 to 0.248. C100B130N40 has the lowest value of $\rho_s f_{yh}/f_c'$ (0.079). This specimen exhibits the least ductile behavior (Fig. 5), while displaying the poorest behavioral parameters (Table 4). Comparing the behavior of the four specimens shows that column ductility increases with the index $\rho_s f_{yh}/f_c'$; however, a careful examination of the results presented in Table 4 indicates that the correlation between $\rho_s f_{yh}/f_c'$ is far from perfect. For example, C100BH80N40 and C100B60N40 have approximately the same $\rho_s f_{yh}/f_c'$ but did not behave similarly (Fig. 4 and 5). Whereas C100B60N40 exhibits a stable ductile behavior up to a ductility of approximately 5, C100BH80N40 behaves in a rather fragile manner with an ultimate displacement capacity of about half that reached by C100B60N40. This is confirmed by the behavioral parameters (Table 4). Moreover, specimen C100BH55N40 has a $\rho_s f_{yh}/f_c'$ value that is about 40% higher than that of C100B60N40. In this case, however, the two columns behave in a very similar manner (Fig. 5) and have comparable behavioral parameters (Table 4). Finally, with specimens C100B130N40, C100BH80N40, and C100B60N40, increasing the index $\rho_s f_{yh}/f_c'$ by about the same value from C100B130N40 to C100BH80N40 or C100B60N40 results in different behavior in the case of C100BH80N40 and C100B60N40, as previously noted.

The second set of specimens presented in Table 4 compares test results obtained for specimens C100BH55N52 and C100B60N52. These two specimens were tested under the same target axial load level of 52%. They behave in a very similar manner as can be seen in Fig. 5, which is further demonstrated by the values of the behavioral parameters (Table 4), even though the $\rho_s f_{yh}/f_c'$ values for the two columns are very different. This corroborates the observations made in the previous paragraph, as Specimen C100BH55N52 and C100B60N52 are identical to Columns C100BH55N40 and C100B60N40 but are tested at a target axial load level of 52%. Comparable results are obtained for these two sets of columns tested at different axial load levels while the $\rho_s f_{yh}/f_c'$ values are quite different.

The third set of columns includes Specimens C120B60N40, C100BH80N40, C80B60N40, and C100BH55N40, all tested at the same target axial load level of 40%. It was shown in the section on the effect of concrete strength that the index $\rho_s f_{yh}/f_c'$ is well-suited for comparing the ductility of columns with different concrete strengths. But when comparing the two pairs of specimens (C120B60N40, C100BH80N40 and C80B60N40, C100BH55N40) having about same $\rho_s f_{yh}/f_c'$ values, the same trend is not evident (Fig. 5). Indeed, Table 4 shows that Specimen C120B60N40, having a confinement index slightly less than Specimen C100BH80N40, has about twice its ductility parameters. The difference is even larger for energy dissipation parameters. The same conclusions can be drawn for Specimens C80B60N40 and C100BH55N40.

The confinement index $\rho_s f_{yh}/f_c'$ takes into account the volumetric ratio of transverse reinforcement ρ_s, the transverse steel yield strength f_{yh}, and the concrete compressive strength f_c'. It is expected that this index would give clear indications to designers about the relative influence that each of these parameters would have on the ductility of columns. For example, the index indicates that the amount of confining steel could be reduced by 50% if the yield strength were doubled. This is the case of Specimen C100B60N40, which has twice as much lateral steel as Specimen C100BH80N40, but with half of its lateral steel yield strength. Contrary to what should be expected for two specimens with the same confinement index, these two columns behave very differently. Measured displacement ductility of C100B60N40 is about twice that of Specimen C100BH80N40; behavioral parameters indicate the same trend. Hence, it is concluded that the confinement index $\rho_s f_{yh}/f_c'$ cannot capture the effect of high-yield-strength confinement steel.

Experimental results demonstrate that a trade-off is possible between the amount and the yield strength of the confinement steel. For example, Specimen C100BH55N40 has 30% less confinement steel than C100B60N40, yet they have comparable behavior. This is achieved by using HYSS in C100BH55N40. In this case, the yield strength is doubled with a concomitant 30% reduction in the volumetric ratio of transverse steel. The same tendency is observed in C100B60N52 and C100BH55N52 with an axial load level of 52%. Because the use of HYSS may be beneficial in certain conditions, it is important to be able to quantify the range of its usefulness.

On columns subjected to concentric compression only, it was experimentally observed that confinement steel does not yield at maximum concrete stress for every column. Hence, it is considered that yield strength is only effective up to a certain limit. This is reflected in the New Zealand Code, which limits the yield strength to 800 MPa. But even this limit would not help with the columns presented here, because the yield strength used is slightly higher than 800 MPa. Cusson and Paultre[12] demonstrated that HYSS is more effective for well-confined columns than columns with poor confinement. Therefore, the effective yield strength should be related to the geometrical distribution and amount of confinement steel provided. This is achieved by the effective confinement index introduced by Cusson and Paultre,[10] which is based on a rational approach to the confinement phenomenon. Based on this work, the effective confinement index is introduced as

$$I_e = \frac{f_{\ell e}}{f_c'} \tag{9}$$

where $f_{\ell e}$ is the effective confinement pressure or the passive pressure applied by the ties to the concrete core when confined concrete reaches its maximum stress. It can be found from horizontal equilibrium

$$f_{le} = K_e \frac{A_{sh}}{cs} f_h' \tag{10}$$

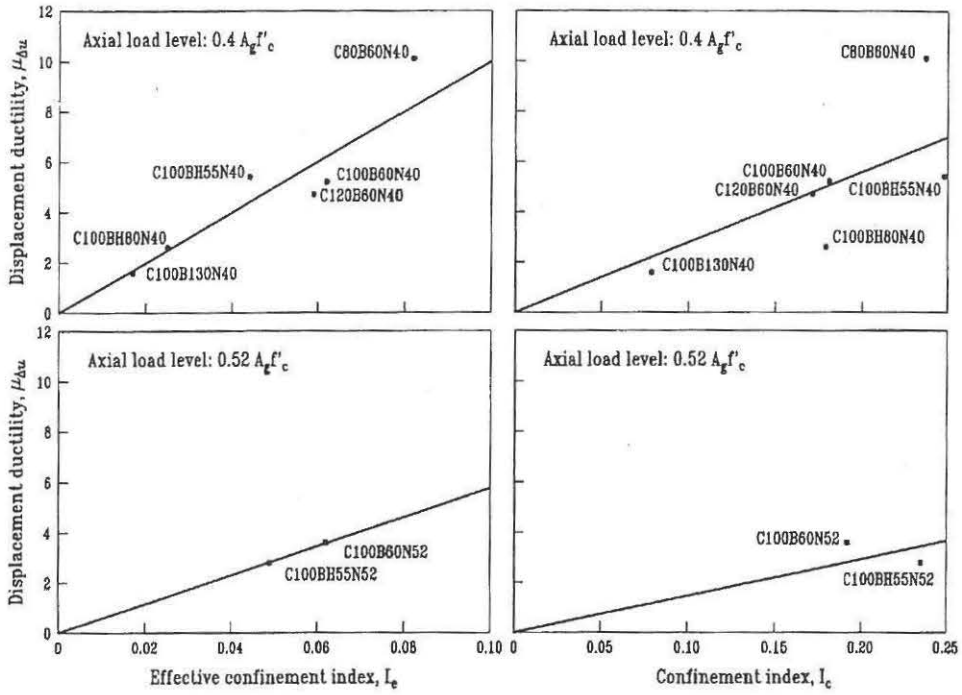

Fig. 10—Influence of effective confinement index on displacement ductility.

where K_e is the geometric coefficient of effectiveness of ties defined by Sheikh and Uzumeri[23] and Mander, Priestley, and Park,[24] A_{sh} is the total confinement steel area in one direction, and f_h' is the stress in the steel at peak. It is seen that the effective confinement pressure accounts for both the distribution of confinement steel and its yield strength. Further discussion of the index can be found in Cusson and Paultre[10] and Paultre and Légeron.[11] Cusson and Paultre[10] demonstrated that this method was very efficient in predicting the effectiveness of the yield strength of lateral steel. The effective confinement index was computed for all the specimens tested in this research program and is reported in Fig. 10, which presents displacement ductility as a function of I_e and I_c. A best-fit line for each axial load level is also presented in this figure. There is very good correlation between the effective confinement index and column ductility at each axial load level. No clear relation between I_c and μ_Δ is apparent from this figure. It can be concluded that the effective confinement index can be used to compare the relative ductility of columns with different concrete strengths and different yield strengths of confinement steel. The relation between I_e and μ_Δ is linear for an axial load level of 40% as with a 52% axial load level. The results of this test program indicate that an index that accounts for the effective confinement index and the level of axial load is the key to understanding the behavior of NSC and HSC columns under cyclic and seismic loads and to developing a general predictive behavioral model.

Requirements for ductility

In seismic zones, structural members designed to behave in a ductile manner should be well-confined. Confinement steel is recommended in codes of practice by design equations. The ACI Code[3] recommends that the total cross-sectional area of rectangular hoop reinforcement shall not be less than

$$A_{sh} = 0.3sh_c\frac{f_c'}{f_{yh}}\left(\frac{A_g}{A_{ch}} - 1\right) \quad (11)$$

and

$$A_{sh} = 0.09sh_c\frac{f_c'}{f_{yh}} \quad (12)$$

where h_c is the cross-sectional dimension of the column core measured center-to-center of confining reinforcement, and A_{ch} is the cross-sectional area of column core measured out-to-out of transverse reinforcement.

Based on the work of Watson, Zahn, and Park,[25] the New Zealand Code[1] recommends an equation that accounts for the axial load level. The minimum effective area of confinement steel in one direction A_{sh} to reach ductile behavior, is obtained from

$$A_{sh} = \frac{\left(1.3 - \rho_g\frac{f_y}{0.85f_c'}\right)sh''}{3.3}\frac{A_g f_c'}{A_c f_{yh}}\frac{P}{\phi f_c' A_g} - 0.006sh'' \quad (13)$$

where h'' is the dimension of the concrete core measured outside the peripheral hoop and ø is the strength reduction factor to be taken as 0.85 for a fully ductile frame building. It should be emphasized that this equation was developed for NSC confined with normal-strength lateral steel. Li, Park, and Tanaka,[5] however, showed that Eq. (13) can be used for HSC confined with normal-strength steel and HYSS, provided that yield strength is limited to a reasonable value. This is accounted for in the New Zealand Code by bounding the yield strength of confining steel to 800 MPa.

Table 5 presents test data for large-scale columns from various authors,[4,5] including test results from the present study. Also included are test data for specimens from this experimental program with normal-strength confinement steel. In this table, the provided effective area of confinement reinforcement A_{sh} is compared with the required reinforcement by the ACI and New Zealand Codes. As there

Table 5—Comparison between provided effective area of confinement reinforcement and required reinforcement by the ACI and New Zealand codes

Specimen	f_c', MPa	s, mm	f_{yh}, MPa	ρ_s	A_{sh}, mm^2	$P/A_g f_c'$	P/P_0	ACI	%ACI	NZS	%NZS	$\mu_{\Delta u}$
U3*	93.0	43	1317	0.0378	227	0.60	0.62	150	151	440	52	1.0
U5*	93.0	62	1317	0.0262	227	0.60	0.62	216	105	635	36	1.0
C100BH80N40†	104.0	80	825	0.0227	242	0.37	0.40	257	94	414	59	2.6
C100BH55N52†	105.0	55	744	0.0330	242	0.53	0.57	197	123	485	50	2.8
D120-15-3C-25/8-0.2P‡	102.0	67	752	0.0255	514	0.19	0.20	335	64	146	146	4.0
C100BH55N40†	110.0	55	825	0.0330	242	0.35	0.38	186	130	286	85	5.4
U1*	98.0	62	1317	0.0262	227	0.30	0.31	228	100	287	79	5.8
D120-15-3C-15/8-0.2P‡	102.0	41	752	0.0413	214	0.19	0.20	208	103	90	238	6.0
C100B130N40†	104.3	130	418	0.0196	341	0.37	0.40	826	41	1233	28	1.6
C100B60N52†	109.4	60	418	0.0426	341	0.51	0.55	400	85	857	40	3.6
C120B60N40†	109.2	60	438	0.0426	341	0.41	0.45	381	90	646	53	4.7
C100B60N40†	98.2	60	418	0.0426	341	0.39	0.42	359	95	565	60	5.2
C80B60N40†	78.7	60	438	0.0426	341	0.40	0.41	274	124	397	86	10.1

*Specimen from Li, Park, and Tanaka.[5]
†Specimen from present research program.
‡Specimen from Azizinamini et al.[4]

is no consensus on the level of ductility to be reached in seismic design and because no single definition of ductility is widely accepted, it was decided to sort the columns in order of increasing ductility and not to separate them into ductile and nonductile columns.

The required confinements differ widely depending on whether Eq. (11) and (12) or Eq. (13) are used. The test results show no correlation between the level of compliance with the ACI Code and the displacement ductility reached. For example, Specimen U1 from Li, Park, and Tanaka[5] behaved quite well and reached a displacement ductility of 5.8, while Specimen U5, with the same ratio of provided transverse reinforcement over required reinforcement by the ACI Code, achieved a displacement ductility of 1.

The overall tendency is well-estimated by the New Zealand Code expressions, as columns with the lower level of compliance with NZS 3101 presented the lowest displacement ductility, while columns with the best level of compliance with NZS 3101 had the highest displacement ductility; however, the correlation is not perfect. For example, Specimen D120-15-3C-25/8-0.2P, tested by Azizinamini et al.,[4] with 146% of steel required by NZS 3101, had lower displacement ductility than Specimen C100BH55N40, with transverse reinforcement equal to 85% of that required by NZS 3101.

One would expect the same level of ductility with the same level of compliance to Eq. (13), regardless of the yield strength of the confinement steel. Hence, specimens with normal-strength confinement steel are included in this discussion to assess this statement. If one compares Specimens C100B60N52, C120B60N40, and C100B60N40 with U3, U5, C100BH80N40, and C100BH55N52 (Table 5), with the level of compliance to the New Zealand Code expression in the same range, the displacement ductility reached is very different: 1 to 2.8 for specimens with high-yield-strength confinement steel and 3.6 to 5.2 for specimen confined with normal-strength steel. Comparison between Specimens C80B60N40 to C100BH55N40 and U1 with compliance to the New Zealand Code expression in the same range shows that the levels of ductility are also very different: 5.4 and 5.8 for columns confined with HYSS and 10.1 for the column confined with normal-strength steel. Hence, we conclude that, even if the level of compliance to the New Zealand Code expression seems to predict quite well the overall tendency of the ductility of the columns confined with HYSS, the level of ductility obtained is very much dependent on the yield strength of the transverse reinforcement.

CONCLUSION

The present study provides data on the behavior of eight HSC columns subjected to combined constant axial compressive load and reversed cyclic flexure. It is shown that the ductility of HSC columns is dependent on concrete strength. It is also demonstrated that the amount of lateral steel can be decreased provided that the yield strength of the lateral steel is increased. Hence, a trade-off exists between yield strength and amount of lateral steel; however, high yield strength may not be effective in every case; when columns are poorly confined, high yield strength is not totally effective and the full yield strength should not be taken into account. Limiting the yield strength of steel to an effective yield strength has not proved effective on the columns tested. This, however, is a simple approach that should be investigated further. The effective confinement index proposed by Cusson and Paultre[12] seems to be a solution to account for HYSS.

Specimens with less confining reinforcement than recommended by the ACI Code behaved in a ductile manner when the axial load was small, while specimens fulfilling the ACI Code expressions for confinement reinforcement did not behave in a ductile manner when the axial load was high. It is also noted that the ACI Code expressions for confinement reinforcement is not applicable to HYSS. The New Zealand Code was tested against eight columns confined with HYSS, including three columns tested in this research program. Some irregularities are observed in the relationship between the level of compliance to the code and the ductility produced. Moreover, the level of ductility reached by columns with similar compliance to the New Zealand Code is different if the column is confined by normal-strength or HYSS. The expressions proposed in the New Zealand Code, however, represent progress compared with the ACI Code

expressions because they account for the axial load level on transverse reinforcement demand, and they limit the yield strength of confining steel to a reasonable value. This aspect, however, needs further study. As long as no improved equations are proposed, the confinement requirements of the New Zealand Code seem more appropriate. There is a possible lack of ductility for columns confined with HYSS. The use of the effective confinement index I_e may be an alternative approach in this case.

A safe and economical use of HSC in seismic zones still depends on relating the available ductility to the confinement reinforcement. When the columns are subjected to high levels of axial load, a high amount of lateral steel is necessary. A ratio of more than 4% will be difficult to use in practice. HYSS is a good way to decrease the amount of transverse reinforcement required, as demonstrated by this research. Hence, design equations should therefore account for such special steel.

ACKNOWLEDGMENTS

The financial assistance provided by the Natural Sciences and Engineering Research Council of Canada (NSERC) and by the Fonds pour la Formation de chercheurs et l'aide à la recherche of the Government of Quebec (FCAR) is gratefully acknowledged.

CONVERSION FACTORS

1 MPa	=	145 psi
1 mm	=	0.0394 in.
1 kN	=	0.2248 kips
1 kNm	=	0.738 ft-kipf

NOTATION

A_c	=	cross-sectional area of the concrete core measured center-to-center of outer tie
A_g	=	gross section of concrete
A_{sh}	=	total cross-sectional area of transverse reinforcement
A_{st}	=	total cross-sectional area of longitudinal reinforcement
E_c	=	secant modulus of elasticity of plain concrete
f_c'	=	maximum compressive strength of concrete measured from 150 x 300 mm cylinders
f_r	=	modulus of rupture of the concrete
f_{su}	=	ultimate strength of reinforcement steel
f_y	=	yield strength of longitudinal reinforcement steel
f_{yh}	=	yield strength of transverse reinforcement steel
H	=	applied horizontal load
H'	=	applied horizontal load H plus the equivalent horizontal load due to P-Δ effect
h'	=	depth of concrete core measured out-to-out of peripheral hoop
P	=	axial load carried by concrete
P_0	=	nominal axial load of a column = $0.85(A_g - A_{st})f_c' + A_{st}f_y$
s	=	center-to-center spacing between sets of ties
Δ	=	tip displacement of column
Δ_2	=	maximum tip displacement of column
Δ_{Iy}	=	ideal yield displacement of column
ε_c	=	axial strain in plain concrete corresponding to f_c'
ε_{sh}	=	commencement of strain hardening in steel bars
ε_{su}	=	ultimate strain of reinforcement steel
ε_y	=	strain in reinforcement steel at yield strength
$\mu_{\Delta u}$	=	ultimate displacement ductility
$\mu_{\phi u}$	=	ultimate curvature ductility
ρ_g	=	volumetric ratio of longitudinal reinforcement in column cross section
ρ_s	=	volumetric ratio of transverse reinforcement in concrete core measured center-to-center of ties
ϕ	=	curvature
ϕ_2	=	maximum curvature
ϕ_{Iy}	=	ideal yield curvature

REFERENCES

1. NZS 3101: Part I, "Code of Practice for the Design of Concrete Structures," Standards Association of New Zealand, Wellington, New Zealand, 1995.

2. CSA Technical Committee, "Design of Concrete Structures for Buildings," CAN3-A23.3-M94, Canadian Standards Association, Rexdale, Ontario, 1994, 199 pp.

3. ACI Committee 318, "Building Code Requirements for Reinforced Concrete (ACI 318-99) and Commentary (ACI 318R-99)," American Concrete Institute, Farmington Hills, Mich., 1999, 391 pp.

4. Azizinamini, A.; Baum Kuska, S. S.; Brungardt, P.; and Hatfield, E., "Seismic Behavior of Square High-Strength Concrete Columns," *ACI Structural Journal,* V. 91, No. 3, May-June 1994, pp. 336-345.

5. Li, B.; Park, R.; and Tanaka, H., "Strength and Ductility of Reinforced Concrete Members and Frames Constructed Using High Strength Concrete," *Research Report* No. 94-5, Department of Civil Engineering, University of Canterbury, Christchurch, New Zealand, 1994, pp. 373.

6. Sheikh, S. A.; Shah, D. V.; and Khoury, S. S., "Confinement of High-Strength Concrete Columns," *ACI Structural Journal,* V. 91, No. 1, Jan.-Feb. 1994, pp. 100-111.

7. ACI-ASCE Committee 441, "High-Strength Concrete Columns: State-of-the-art," *ACI Structural Journal,* V. 94, No. 3, May-June 1997, pp. 323-335.

8. Bayrak, O., and Sheikh, S. A., "High-Strength Concrete Columns under Simulated Earthquake Loading," *Journal of Structural Engineering,* ASCE, V. 124, No. 9, 1998, pp. 999-1010.

9. Légeron, F., and Paultre, P., "Behavior of High-Strength Concrete Columns Under Cyclic Flexure and Constant Axial Load," *ACI Structural Journal,* V. 97, No. 4, July-Aug. 2000, pp. 591-601.

10. Cusson, D., and Paultre, P., "Stress-Strain Model for Confined High-Strength Concrete," *Journal of Structural Engineering,* ASCE, V. 121, No. 3, 1995, pp. 468-477.

11. Paultre, P., and Légeron, F., "Seismic Behavior of High-Strength Concrete Tied Columns," *High-Strength Concrete, Proceedings of the First International Conference*, A. Azizinamini, D. Darwin, and C. French, eds., ASCE, Reston, Va., 1999, pp. 159-172.

12. Cusson, D., and Paultre, P., "High-strength Concrete Columns Confined by Rectangular Ties," *Journal of Structural Engineering,* ASCE, V. 120, No. 3, 1994, pp. 783-804.

13. Khayat, K.; Tremblay, S.; and Paultre, P., "Structural Response of Self-Consolidating Concrete Columns," *Self-Compacting Concrete,* Proceedings of the First International RILEM Symposium, A. Skarendahl and O. Petersson, eds., Sept. 13-14, 1999.

14. Paultre, P.; Khayat, K.; Langlois, Y.; and Trudel, A., "Structural Performance of Some Special Concretes," *4th International Symposium on High Performance Concrete Utilization*, Paris, ENPC, 3, 1996, pp. 787-796.

15. Watson, S., and Park, R., "Simulated Seismic Load Tests on Reinforced Concrete Columns," *ASCE Journal of the Structural Division,* V. 120, No. 6, 1994, pp. 1825-1849.

16. Sheikh, S. A., and Khoury, S. S., "Confined Concrete Columns with Stubs," *ACI Structural Journal,* V. 90, No. 4, July-Aug. 1993, pp. 414-431.

17. Tanaka, H.; Park, R.; and McNamee, B., "Anchorage of Transverse Reinforcement in Rectangular Reinforced Concrete Columns in Seismic Design," *Bulletin of the New Zealand National Society for Earthquake Engineering,* V. 18, No. 2, June 1985, pp. 165-190.

18. Paultre, P.; Légeron, F.; and Mongeau, D., "Behavior of High-Strength Concrete Columns—Influence of Concrete Strength and Transverse Reinforcement Yield Strength," *Research Report* CRGP-00/02, Department of Civil Engineering, Université de Sherbrooke, Sherbrooke, Québec, 50 pp.

19. Newmark, N. M., and Hall W. J., *Earthquake Spectra and Design,* Earthquake Engineering Research Institute, Berkeley, Calif., 1980, 103 pp.

20. Park, R., "Evaluation of Ductility of Structures and Structural Assemblages from Laboratory Testing," *Bulletin of the New Zealand National Society for Earthquake Engineering,* V. 22, No. 3, 1989, pp. 155-166.

21. Gosain, K. N.; Brown, H. R.; and Jirsa J. O., "Shear Requirements for Load Reversals on RC Members," *ASCE Journal of the Structural Division,* V. 103, No. 7, 1977, pp. 1461-1476.

22. Ehsani, M. R., and Wright, J. K., "Confinement Steel Requirements for Connections in Ductile Frames," *ASCE Journal of the Structural Division,* V. 116, No. 3, 1990, pp. 751-767.

23. Sheikh, S. A., and Uzumeri, S. M., "Analytical Model for Concrete Confinement in Tied Columns," *ASCE Journal of the Structural Division,* V. 108, No. 12, 1982, pp. 2703-2722.

24. Mander, J. B.; Priestley, M. J. N.; and Park, R., "Seismic Design of Bridge Piers," *Research Report* No. 84-2, University of Canterbury, Christchurch, New Zealand, 1984.

25. Watson, S.; Zahn, F. A.; and Park, R., "Confining Reinforcement for Concrete Columns," *Journal of the Structural Division,* ASCE, V. 120, No. 6, 1994, pp. 1798-1824.